RESEARCH

Thermomechanical characterisation and plane stress linear viscoelastic modelling of ethylene-tetra-fluoroethylene foils

Alessandro Comitti[1,2] · Federico Bosi[1,3]

Abstract

Ethylene-tetra-fluoroethylene (ETFE) is a polymer employed in tension membrane structures with mechanical properties that strongly depend on time and temperature effects. A comprehensive understanding of the mutual influence of these variables and a unified viscoelastic constitutive model design can enable wider exploitation of ETFE in sustainable lightweight construction. This study presents a thermomechanical characterisation of ETFE foils through quasi-static tensile experiments spanning two orders of magnitude of strain rates, creep, relaxation, shear and dynamic cyclic tests in a wide range of temperatures suitable for building applications, from $-20°$ C to $60°$ C. The experimental results in different material orientations are used to identify the limits of the linear viscoelastic domain, define the direction-dependent creep compliance master curves and calibrate the parameters of a plane stress orthotropic linear viscoelastic model, employing the Boltzmann superposition and the time-temperature superposition principles. The model has been numerically implemented using a recursive integration algorithm and its code is provided open source. A validation on independently acquired data shows the accuracy of the constitutive model in predicting ETFE behaviour within the linear viscoelastic regime usually adopted during structural design, with excellent extrapolation capabilities outside the range of the calibration data.

✉ F. Bosi
f.bosi@ucl.ac.uk

A. Comitti
a.comitti@ucl.ac.uk

1 Department of Mechanical Engineering, University College London, Torrington Place, London, WC1E 7JE, UK

2 CAEmate s.r.l, Via Alessandria 15, Bolzano, 39100, Italy

3 Department of Innovative Technologies, University of Applied Sciences and Arts of Southern Switzerland, Via la Santa 1, Lugano-Viganello, 6962, Switzerland

1 Introduction

Ethylene-tetra-fluoroethylene (ETFE) has been used in the construction industry since 1970, when the material started to be produced in foils to be installed in roof construction of greenhouses. Over time, the popularity of ETFE among designers and builders has grown substantially, mostly due to its architectural value, mechanical properties, and the possibility to be adapted to complex envelope designs. Some recent examples are the Shed at Hudson Yards in New York City (2021), the U.S. Embassy in London (2017), and the 'Water Cube' in Beijing (2008). The structural interest in ETFE is well justified by its high transparency, mechanical strength, stiffness and ductility, UV and chemical agents resistance, self-extinguishing properties, recyclability, and lightness of around 350 g/m^2 for a typical 200 μm foil (Hu et al. 2017). The material is especially convenient for building claddings and envelopes to target sustainable development in the built environment (Comitti et al. 2024).

ETFE mechanical behaviour shows an almost tri-linear response with two distinct inflection points in a typical uniaxial stress-strain plot (Galliot and Luchsinger 2011). Similar to polyethylene (De Focatiis and Gubler 2013), the first point is assumed to be related to yielding of the amorphous phase and rotation of crystals, while the second transition marks the irreversible damage of the crystalline phase (Brooks et al. 1992). ETFE is a stiff thermoplastic that exhibits great ductility, reaching up to 4–500% engineering strain at failure (De Focatiis and Gubler 2013). The polymeric nature of the material implies a viscous behaviour with time and temperature dependence, confirmed by many contributions to the literature. Galliot and Luchsinger (2011) performed uniaxial tensile tests at different strain rates in the range 0.4 to 200%/s at ambient temperature. This showed an increase of 20% in the initial stiffness, and of 40% on the yield stress (assumed as the first inflection point) when the deformation rate was increased from the lowest to the highest. The effects of temperature were shown to be even more relevant, producing a decrease in properties between ambient temperature and 60° C, amounting to 47% for the stiffness and 58% for the yield strength (Hu et al. 2015). However, different experimental campaigns have shown large variability in the measurements and mechanical properties (Hu et al. 2015), attributed to the lack of uniformity in the testing procedures, the foil thicknesses and the foil manufacturer (Surholt et al. 2022). De Focatiis and Gubler (2013) also experimentally investigated the influence of the material's orientation on its response. The extrusion (or machine, MD) direction of the material and the transverse direction (TD) were shown to have slightly different behaviour, inconsistent across the tested thickness range and among foil producers.

Li and Wu (2015) carried out uniaxial creep-recovery tests to develop a nonlinear viscoelastic response based on the theory proposed by Schapery (1969). Yoshino and Kato (2013, 2016, 2017, 2019) followed a similar approach based on the Prony series representation of the material compliance through a generalised Kelvin model (Brinson and Brinson 2008), adding some stress-dependent factorisation to account for nonlinearities. However, both constitutive relations work only for a limited number of cases, while other models (Surholt et al. 2022; Beck 2021) are unable to predict ETFE time-dependent response accurately. The aforementioned uncertainties result from a deficiency of standards to guide the design process and verification of lightweight ETFE membrane structures. Pending a comprehensive standard on the design of tension structures (Stranghöner et al. 2016), one of the most valuable documents to date is provided by Tensinet (Houtman 2013), which summarises different contributions from the literature to describe and model ETFE response. Moreover, design advice for ETFE membrane structures is provided, suggesting the use of a linear elastic model, with the stiffness values changing according to the load case. In particular, two different elastic moduli are provided for short and long loading times. However,

as Cabello and Bown highlighted in their contribution (Cabello and Bown 2019), the development of a reliable thermo-viscoelastic constitutive model is needed to achieve a confident design of ETFE structures. In their work, the authors re-factored a model developed by Bosi and Pellegrino (2018) to match some ETFE experimental data and applied it to common loading scenarios for membrane structures. The comparison between those results and guideline recommendations (Houtman 2013) shows how the design of ETFE is currently inaccurate and often unsafe. The latest effort for standardisation, the FprCEN/TS 19102:2023 (European Commission et al. 2023), contains additional useful information about the structural design with these foils, but still does not include comprehensive provisions on how to account for the time- and temperature-dependent behaviour.

The current research aims to foster ETFE design by performing a unique and comprehensive thermomechanical characterisation in a wide range of loading conditions, material orientations, temperatures from $-20°$ C to $60°$ C and deformation rates from 0.01%/s to 1%/s. The unique combination of measured data enables the (i) identification of the limit of the linear viscoelastic domain, (ii) the determination of the creep-compliance master curves for ETFE in different material directions through the time-temperature superposition principle (TTSP) and (iii) the definition of a comprehensive orthotropic time- and temperature-dependent model that combines several approaches from polymer viscoelasticity to predict uniaxial, creep and relaxation behaviour with a single law. The paper is organised as follows: Sect. 2 describes the procedures employed to characterise ETFE foil, which includes quasi-static, dynamic and creep tests, while Sect. 3 presents the analysis and discussion of the results of the experimental campaign. The development of an orthotropic linear viscoelastic modelling, its numerical implementation in a finite element material subroutine and its validation are shown in Sect. 4.

2 Materials and methods

This section presents the experimental campaign carried out to characterise the thermomechanical response of ETFE membranes. The material employed is a 200 μm thick foil produced by Nowofol (ET6235Z), which is widely used in civil engineering applications. The structural film is manufactured by extruding the polymeric resin along the machine direction (MD), while its orthogonal direction is labelled as transverse direction (TD). The specimens were laser cut to obtain flawless edges and high accuracy in the sample dimensions, according to the requirements for thin film testing. Different cutting methods were tested, including laser cut, die and razor, with the former that resulted the most reliable and accurate technique without affecting the mechanical results.

2.1 Uniaxial dynamic tests

A Dynamic Mechanical Analyser (DMA) from TA Instruments (Discovery DMA 850), equipped with tensile clamps, was used to carry out dynamic uniaxial tensile tests at various frequencies and amplitudes at controlled temperatures, Fig. 1a. The specimens were laser cut to a width of 5.5 mm and a length of 18 mm.

The test procedure consisted of cyclic tests performed at an amplitude of 0.1% strain while the temperature was ramped from $-150°$ C to $150°$ C at a rate of $3°$ C/min, for MD direction only. This procedure was repeated at frequencies of 0.1, 1 and 10 Hz to investigate the transitions in the polymeric material and their variations in the frequency domain.
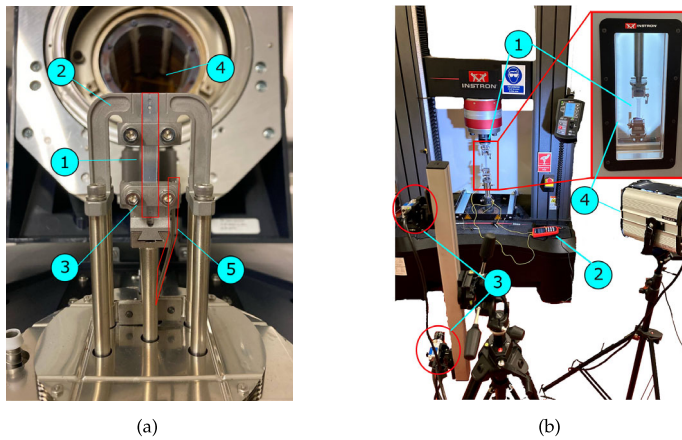
(a)   (b)

Fig. 1 Experimental setups: (a) an ETFE specimen (1) placed in the DMA, clamped between the fixed clamp (2) and the movable shaft (3). The furnace (4), once closed, allows the temperature control through a thermocouple (5); (b) uniaxial tensile test, composed by an electromechanical testing machine with the clamped specimen (1), temperature reader (2), stereo DIC cameras (3) and LED lights (4). When the temperature was controlled, the test was executed within an environmental chamber. (Color figure online)

2.2 Uniaxial tensile tests

An Instron 5985 equipped with a 2530-500 N load cell and 2713-004 self-tightening roller grips were utilised, as shown in Fig. 1b. To control the temperature, a 3119-606 Instron environmental chamber was used, cooled by LN_2. Additionally, a two channels Omega HH801A meter was employed to record the temperature in the proximity of the specimens with two thermocouples type K. The engineering stress was computed from the force recorded by the load cell.

The measurement of the kinematic fields (strains and displacements) was performed using Digital Image Correlation (DIC) (Sutton et al. 2009). The stereo system is composed of two digital cameras Basler acA2440 75 μm 5.0 MP, equipped with Schneider Kreuznach Xenoplan 1.9/35 mm lens. The images were acquired through VICSnap 9.0 (Correlated Solutions) and processed by VIC3D 8.0 (Correlated Solutions) to compute the motion of the specimen from the initial reference image. The stereo system was calibrated by acquiring pictures of a calibration plate (14×10 dots grid, with a spacing of 7 mm) in different positions and tilt angles from the test reference plane. The goal was to obtain a calibration score lower than 0.03 pixels to achieve good accuracy, with a minimum of 30 images per camera. The specimens were laser cut according to the dimensions indicated in ASTM D412 (2021), type 'A' die (D11 Committee 2021). For DIC measurements, each specimen was spray painted with Rust-Oleum 330505 universal black paint (matte effect) to create a random speckle pattern. An external LED light was used to obtain adequate light conditions and enhance the contrast between the transparent specimen and the black speckles. When the environmental chamber was employed and light reflections on its external glass might have affected the quality of the images, a custom aluminium frame, equipped with a light-diffusing panel and adhesive strips of LED lights, was placed behind the specimen. In the image post-processing phase, the correlation subset was 29×29 pixels, with a step size of 7 pixels and a filter size of 15 pixels (Solutions 2019). Through DIC, the average and maximum engineering strains were measured in the gauge length of the specimens. The

deviation between these two strain values was found negligible up to the second inflection point. Hence, since this work focuses on the characterisation and modelling of the linear viscoelastic region, only the average strain across the gauge area is considered in the following.

Time and temperature effects have been investigated to assess the viscous response of ETFE. In particular, uniaxial tensile tests at different strain rates, namely 0.01%/s, 0.1%/s, and 1%/s, were performed. The aimed strain rates were reached by imposing a constant displacement rate of the machine crossbar of 0.55, 5.5, and 55 mm/min, respectively. This test procedure was executed at ambient temperature $T_{amb} = 23°$ C $\pm 1.5°$ C and at T $= -20°$ C, $0°$ C, $40°$ C, and $60°$ C. In the experiments executed at temperatures other than T_{amb}, the specimens experienced a soak phase of 15 minutes once the prescribed temperature condition was reached. To avoid any thermal dilatation/contraction influence on the results, the specimens were left slack while reaching the set temperature and during the soak. Both MD and TD directions were tested to assess any orthotropic effect. Moreover, specimens cut at an angle of 45° from MD (or TD) direction were tested to characterise the in-plane shear behaviour, by rotating the stress and strain tensors from the uniaxial loading direction to the material principal axes analogous to Li et al. (2016). This choice was made in order to characterise the in-plane shear properties of the ETFE membrane without performing simple or pure shear tests that would be ineffective because they introduce wrinkling instability (Wong and Pellegrino 2006). This direction will be called Inclined Direction (ID) in the following, and only the shear strain and stress will be plotted. Statistical significance is considered to be achieved with a minimum of three samples tested, from which an average curve and standard deviation were computed. This procedure allowed a deep investigation of time and temperature effects across two strain rate orders of magnitude, and in a temperature range typical for civil engineering applications.

2.3 Creep tests

Uniaxial creep tests at different stress levels were performed with the DMA to investigate the nonlinearity of ETFE behaviour and to identify the boundaries of the linear viscoelastic region. Short-term creep tests lasted 30 min, with the same specimen preparation and test equipment described in Sect. 2.1. Considering the quasi-isotropic response of ETFE at small strain reported in the literature (Galliot and Luchsinger 2011), only samples cut along MD were tested. The stress levels tested were 0.6, 1, 1.3, 1.5, 2 and 3 MPa at a temperature of $60°$ C, where the nonlinearities are expected to be more relevant. The relatively small creep strains achieved are caused by the selected test duration and the stresses investigated, which are comparable to those experienced by ETFE foils employed in building applications and considered when designing such structures for serviceability state.

Subsequently, given that 1.5 MPa was determined to be the threshold stress at which nonlinearities occur at $60°$ C (see also Sect. 3.3), uniaxial creep tests were performed with the DMA at different temperatures in the range -20 to $65°$ C, with an interval of $5°$ C and $10°$ C above and below $0°$ C respectively. Such creep tests lasted 4 hours and three material directions were considered, i.e. MD, TD and ID. The creep stress was reached with a 210 MPa/min ramp ($\sim$0.5 s), assuring a quasi-instantaneous loading condition. The first 120 s of the data were discarded to remove the data that might have been affected by the dynamic effects introduced by the fast loading ramp.

Fig. 2 Uniaxial dynamic tests performed along MD at 0.1, 1, and 10 Hz, with a strain amplitude $\bar{\epsilon} = 0.1\%$ and temperature ramping at a rate of $3°$ C/min. The ellipse highlights a secondary transition occurring within the temperature range of interest, delimited by vertical dashed lines. (Color figure online)
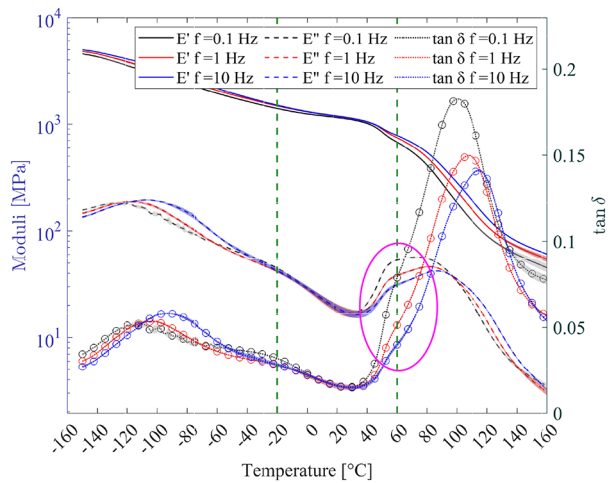
3 Experimental results and discussion

3.1 Uniaxial dynamic tests

Figure 2 reports the real and imaginary counterparts of the complex modulus, the storage E' and the loss E'' moduli. They represent the stored (elastic) and dissipated (viscous) energy of the material, respectively. Moreover, the plot shows the ratio between the two, also known as the phase angle $\tan\delta$, which represents the lag in the response of the material due to viscous effects. According to the classic definition of the glass transition temperature, T_g, as the temperature at the peak of $\tan\delta$, the value found for ETFE is between $100°$C and $120°$ C, depending on the frequency. Alternative definitions, such as the temperature at the peak of the loss modulus or midway through the steep decrease of the storage module, would define a wider region between $80°$ C and $120°$ C. Nevertheless, in the range of temperatures considered in this study ($-20°$ C to $60°$ C), ETFE is in its glassy phase.

Additionally, a secondary transition can be recognised as local maxima of the curves representing the dynamic moduli and $\tan\delta$, as highlighted in the magenta ellipse in Fig. 2. In the range of temperatures of interest, a transition can be observed beyond $40°$ C. This transition influences the behaviour of ETFE and could affect the material time-temperature relation. Hence, difficulties may emerge in the application of the time-temperature superposition because of the change in the slope of the moduli curves. This consideration will be further addressed in Sect. 3.3, where the time-temperature superposition principle is applied to creep tests.

3.2 Uniaxial tensile tests

Similar to literature data, Fig. 3 shows that ETFE's response is characterised by two changes of slope, which define two inflection points. They are assumed to be caused by the yielding of the amorphous phase and permanent damage of the crystalline phase, respectively (Brooks et al. 1992; De Focatiis and Gubler 2013). To make preliminary quantitative comparisons between the test results at different temperatures and deformation rates in the region of interest for structural applications (i.e. before the onset of plasticity), the initial modulus E was obtained from a linear regression analysis of the stress-strain curves (Hu et al. 2015;

Fig. 3 Orientation effects on ETFE engineering stress-strain curve at $T_{amb} = 23°$ C and variation of the initial stiffness as a function of the temperatures and strain rates investigated (inset) as $(E_{MD} - E_{TD})/E_{TD}$. The solid line represents the average value, while the coloured area is the standard deviation. (Color figure online)
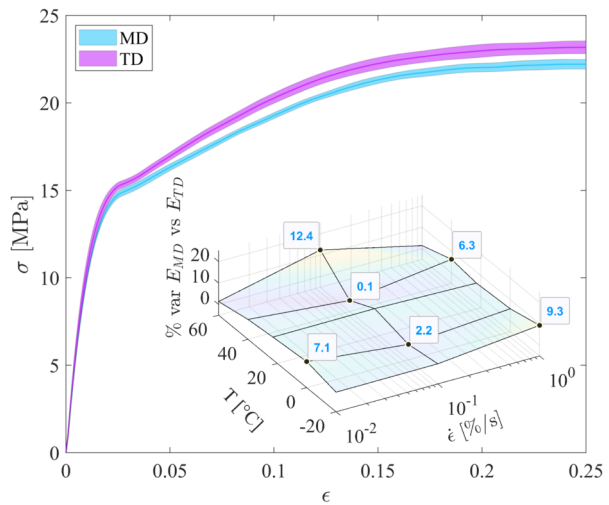
Sun et al. 2022). It should be noted that although such mechanical property indicates a temperature and strain rate dependency of ETFE, it will not be employed in the definition of a comprehensive rheological material model, Sect. 4.

Orientation effects are shown Fig. 3, where the stress-strain response in the two principal directions MD and TD are compared in sets of tests executed at ambient temperature and a strain rate of 0.1%/s. In the same figure, the inset displays the initial stiffness variation with respect to the response at 0.1%/s in the domain of temperatures tested. The material shows a limited orthotropy at small strains, which increases at larger deformations, with TD always stiffer than MD. In particular, the maximum stiffness variation between the two material directions is 12% and was observed in the tests with a strain rate of 0.1%/s and a temperature of 60° C, while all other uniaxial tests presented lower stiffness variations with an average value of 5%. Although the material anisotropy is limited, especially at small strains, the constitutive linear viscoelastic model will be developed as orthotropic to make it as accurate as possible and to be able to expand it to nonlinear and viscoplastic domains, where orthotropy effects are more pronounced. Please note that Fig. 3 reports the mechanical response until 25% engineering strain to highlight the behaviour of ETFE until large strains. However, in the following, the attention will be restricted to smaller strains to highlight the viscoelastic regime representative of ETFE design when used in building applications.

An example of the deformation rate effect on the material response is shown in Fig. 4 for tests carried out at 20° C along MD. The plot shows that the strain rate has a limited influence on the mechanical response, mainly affecting the yield point's magnitude and shifting the post-viscoelastic region vertically. TD and ID directions presented analogous results, reported in Appendix A for the sake of brevity. To provide a quantitative comparison, the strain rate of 0.1%/s was taken as a reference. As expected from polymers' behaviour, the initial modulus E increases with faster deformation rates, while slower stain rates decrease it. The strain rate of 1%/s has an average stiffening effect of 2% (considering all uniaxial tests executed), while 0.01%/s strain rate decreases E of 6% on average. The inset of Fig. 4 displays the variation of initial stiffness for the fastest and slowest strain rates compared to 0.1%/s, showing that at higher temperatures, strain rate effects have a more pronounced effect. Temperature effects are shown in Fig. 5, where the strain rate of the tests is the same among the samples. The effects of temperature are evident, and to give a quantitative comparison, the

Fig. 4 Strain rate effects on ETFE engineering stress-strain curve at $T_{amb} = 23°$ C and along MD. The inset shows the percentage variation of the initial stiffness E with respect to that at the reference strain rate 0.1%/s for every temperature tested as $\left(E_{\dot{\epsilon}} - E_{0.1\%/s}\right)/E_{0.1\%/s}$. The solid line represents the average value, while the coloured area is the standard deviation. (Color figure online)
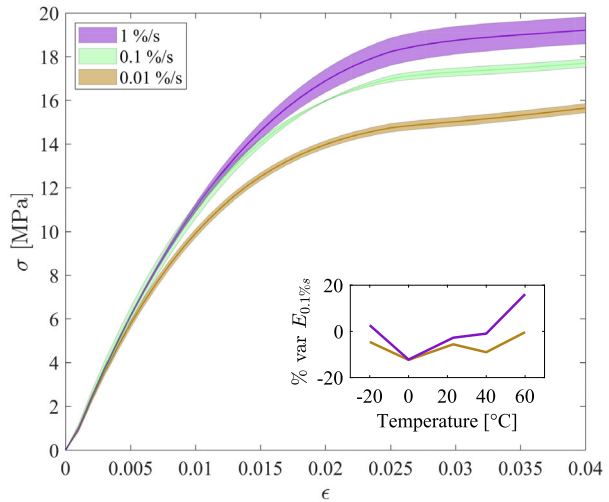
Fig. 5 Temperature effects on ETFE engineering stress-strain curves at 0.1%/s strain rate along MD. The inset shows the percentage variation of the initial stiffness E with respect to that at the ambient temperature $T_{amb} = 23°$ C, for every strain rate tested as $\left(E_T - E_{T,amb}\right)/E_{T,amb}$. The solid line represents the average value, while the coloured area is the standard deviation. (Color figure online)
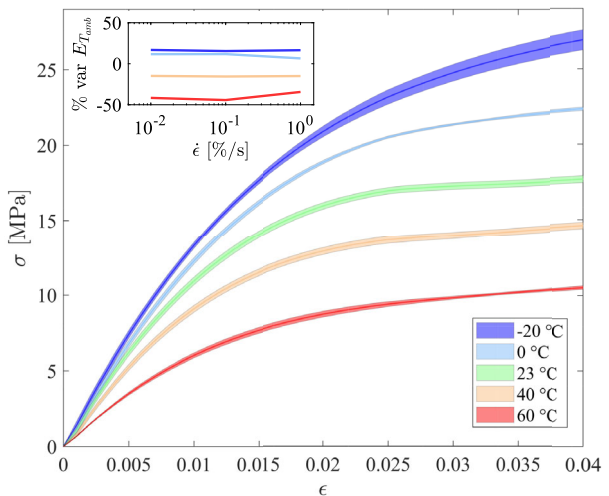
ambient temperature tests were taken as a reference. For what concerns the initial modulus E, low temperatures cause an increase in its magnitude, opposite to the effect of higher temperatures. The average increase in initial stiffness observed at 0° C across the strain rate range tested is 5% for MD, reaching an average increase of 15% across all tests performed at $-20°$ C. Similar effects can be observed at higher temperatures, where an average decrease of 16% and 41% are recorded at 40° C and 60° C and, respectively. Analogue variations were found for TD and ID directions, as shown in Appendix A. Similar to stiffness, the onset of plasticity is highly influenced by temperature, as it can be observed from the same plot, regardless of the method employed to calculate the yield point. The relevance of the temperature effects on the material response and the potential undesired consequences for its inadequate modelling are evident, including water ponding or wind-induced fluttering on ETFE structures (Houtman 2013).

Table 1 Initial stiffness E of ETFE from uniaxial tensile tests reported as a function of the strain rate, temperature and material direction

$\dot{\epsilon}$ [%/s]	T [° C]	E		
		MD [MPa]	TD [MPa]	ID [MPa]
0.01	−20	1338.85	1396.58	932.99
	0	1279.69	1377.91	890.26
	23	1145.88	1213.98	821.41
	40	975.65	1019.09	672.36
	60	668.85	678.04	408.63
0.1	−20	1408.75	1472.88	962.02
	0	1363.58	1393.61	961.05
	23	1219.90	1295.99	837.03
	40	1030.02	1028.89	689.14
	60	679.87	775.91	502.46
1	−20	1402.70	1546.37	939.09
	0	1282.53	1360.97	907.03
	23	1203.88	1264.32	910.62
	40	1023.28	1091.99	702.61
	60	790.15	778.90	490.77

Overall, it can be concluded that the material is slightly orthotropic, the strain rate effect has a minor influence on the initial stiffness (at the rates tested), while temperature has a great impact on the mechanical response. Table 1 reports the initial stiffness calculated for the different conditions tested.

3.3 Creep tests and linear viscoelastic domain

The results of short-term creep tests at 60° C are shown in Fig. 6, where isochrone points for different stress levels are displayed at the last time instant of the test, i.e. 30 min. The construction of the isochrones plot is generated according to Brinson and Brinson, Sect. 3.4.3. From the isochrones, the compliance (or stiffness) is independent of the stress/strain if the ratio between stress and strain is proportional across different stress levels, thus suggesting a linear viscoelastic response. Figure 6 also reports a linear fit of the isochrone data points until a creep stress of 1.5 MPa. To account for uncertainties, a similar regression procedure was performed considering the standard deviation of the samples, producing the blue-coloured area in Fig. 6. In the isochrone plot, the material starts to deviate from a linear behaviour at 2 MPa. Hence, ETFE's linear viscoelastic limit from creep tests is set at 1.5 MPa.

Subsequently, 4 hours creep tests at 1.5 MPa and various temperature conditions were executed to characterise the linear viscoelastic region of ETFE, in all three directions (MD, TD, ID). From the tests, the temperature- and time-dependent creep compliance $D(t)$ was measured, as shown for MD in Fig. 7 (left). With these data, the time-temperature superposition principle (TTSP) was applied to build a creep-compliance master curve for each direction tested. The reference temperature for the TTSP was chosen as $T_{ref} = 20°$ C as the midspan of the temperature range considered and similar to ambient temperature. A horizontal shift of all curves, except from the one at the reference temperature, was performed, aiming to create a smooth experimental master curve by means of aligning the starting point of each sample's compliance to the neighbour curve (Ward 2013). Data from tests performed

Fig. 6 Creep tests isochrones at $t = 30$ min, T $= 60°$ C, MD
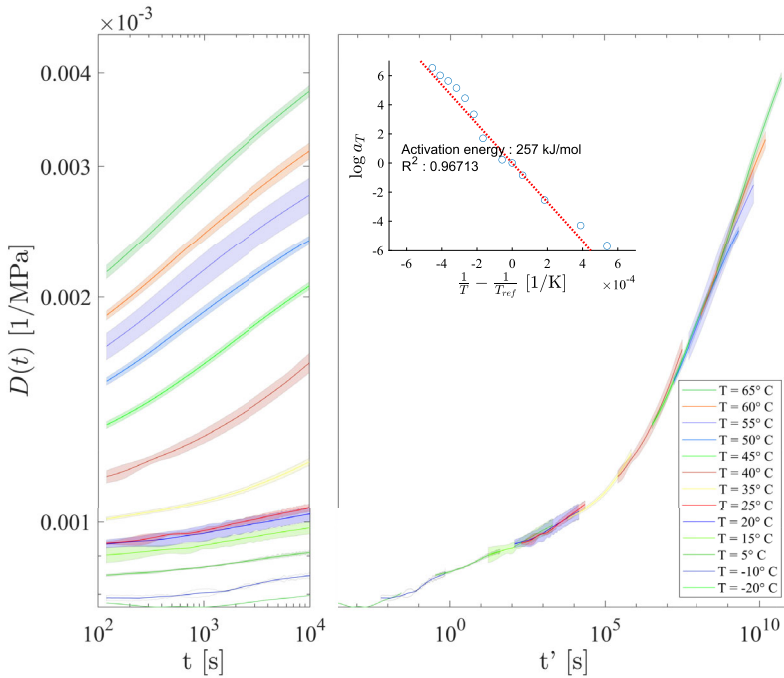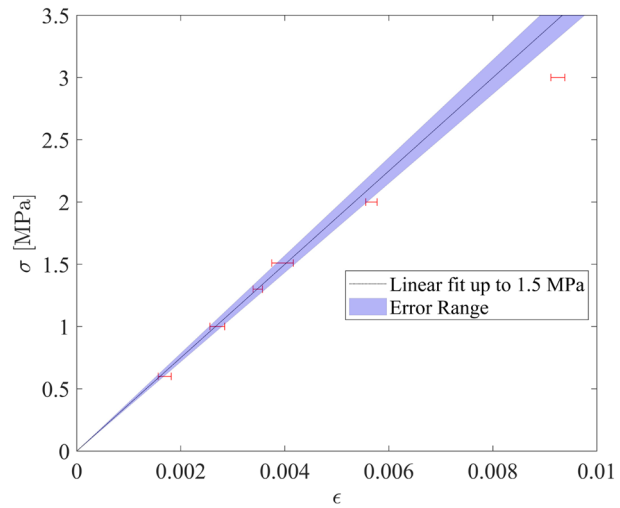

Fig. 7 Left: engineering creep compliance at different temperatures from creep test performed at $\sigma_0 = 1.5$ MPa along MD. Right: Engineering creep compliance master curves along MD at $T_{ref} = 20°$ C, obtained by horizontally shifting the compliance curves at other temperatures through the time shift factor a_T. The inset shows the experimental shift factors and their fitting through the Arrhenius law. (Color figure online)

at T $<$ T_{ref} and T $>$ T_{ref} were shifted to the left and right in the time scale, respectively. The shifting operation can be quantified by the shift factor a_T, which depends only on the tem-

perature for linear viscoelasticity. It enables to simulate the response of the material for shorter and longer times by scaling the time and obtaining a reduced time $t' = \dfrac{t}{a_T}$ for non-isothermal conditions (Schapery 1969).

The resulting experimental master curve at the reference temperature and in the reduced time domain is shown in Fig. 7 (right). Similar results were obtained for directions TD and ID, shown in Figs. B1 and B2 in Appendix B, respectively. A pronounced change in the slope of the master curve can be observed above ca. 40° C, resembling the typical increase of the S-shaped master curves of polymers. Additionally, above that temperature, it seems that the compliance curves should also be rotated to superimpose with the others. This effect, which underlies a modification of the relations between time and temperature and a faster viscous response, is assumed to be associated with the secondary transition observed in Fig. 2. Although some attempts exist (Fesko and Tschoegl 2007), to date, no shift factor equation captures such rotation. In the literature, similar discrepancies were observed in the construction of the master curves and were disregarded when applying the TTSP (Li et al. 2016).

Since ETFE is in its glassy phase in the temperature range of interest, the Arrhenius law was fitted to the experimentally-derived time shifts a_T (Arrhenius 1889). The Arrhenius law describes the rate of a temperature-activated deformation process, where molecules have to overcome an energy barrier to move from one state to another. The height of the energy barrier is constant and defined as the activation energy E_a, while different temperature conditions modify the energy of the initial state. Following this theory, the relaxation time can be expressed as

$$\tau = A e^{\frac{-E_a}{RT}},\tag{1}$$

where R is the universal gas constant and A is a material parameter. Comparing the logarithms of the relaxation times τ at a generic temperature T and at the reference temperature T_{ref}, the expression of the shift factor results

$$\log_{10} a_T = \log_{10} \frac{\tau(T)}{\tau(T_{ref})} = -\frac{E_a}{2.303R}\left(\frac{1}{T} - \frac{1}{T_{ref}}\right).\tag{2}$$

In this work, a linear interpolation of the time shifts $\log a_T$ was performed according to Equation (2), determining the parameter E_a associated with each of the three master curves created and imposing no shift at T_{ref}. The time-temperature superposition through the Arrhenius law well describes ETFE linear viscoelastic response, as shown in the inset of Fig. 7 (right). It can be observed that, at higher temperatures, the horizontal shifts start to deviate more from the Arrhenius regression. This is associated with the secondary material transition, occurring at temperatures sufficiently close to the glass transition. Nevertheless, such minor deviation of the shift factors from the fitted Arrhenius law does not significantly affect the accuracy of the linear viscoelastic modelling or its results, as will be shown in the following sections. For the modelling of the time-temperature superposition, reported in the following section, a single activation energy, $E_a = 260.7$ kJ/mol, was taken as the average of the activation energies obtained from the fitting of the three master curves along MD, TD and ID, Table 2. A single activation energy can also be determined by fitting altogether the shift factors determined in MD, TD and ID, providing a very similar result with only a +0.3% difference.

4 Linear viscoelastic modelling

4.1 Plane stress orthotropic constitutive model

The measured experimental data were used to build and validate a rheological model. In particular, the creep test master curve in Fig. 7 (right) was used to create a linear viscoelastic model. Given the nature of the investigated material, which is produced for and employed in buildings as a thin foil with negligible bending stiffness, an orthotropic plane stress formulation (Karwath et al. 2007) is considered. Adopting the Boltzmann superposition principle for a generalised Kelvin element (Brinson and Brinson 2008), the mechanical strain tensor can be expressed through the following plane stress viscoelastic constitutive relation

$$\boldsymbol{\epsilon}(t) = \int_0^t \boldsymbol{D}(t-s)\frac{d\boldsymbol{\sigma}}{ds}\, ds, \tag{3}$$

where $\boldsymbol{\epsilon} = [\epsilon_1, \epsilon_2, \epsilon_6]^{\mathrm{T}}$ and $\boldsymbol{\sigma} = [\sigma_1, \sigma_2, \sigma_6]^{\mathrm{T}}$ are the time-dependent engineering strain and stress vectors, respectively, and s is the integration variable. A small strain formulation was chosen because the linear viscoelastic regime was found to be valid until ca. 1% of strain, at which point the differences between engineering and large strain measures are negligible. Furthermore, ETFE is employed in engineering applications mainly as a building cladding foil, whereby such small strain limits are representative of the serviceability design. The in-plane normal directions 1 and 2 correspond with MD and TD respectively, while 6 represents the shear component along ID. $\boldsymbol{D}$ is the symmetric creep compliance matrix

$$\boldsymbol{D} = \begin{bmatrix} D_{11} & D_{12} & 0 \\ D_{21} & D_{22} & 0 \\ 0 & 0 & D_{66} \end{bmatrix}. \tag{4}$$

Each compliance term D_{jk} is represented by a Prony series as

$$D_{jk} = D_{jk,0} + \sum_{i=1}^{N} D_{jk,i}\left(1 - e^{-\frac{t-s}{\tau_i}}\right), \tag{5}$$

where $j, k = \{1, 2, 6\}$, $D_{jk,0}$ is the instantaneous compliance of an ideal spring added to the series of N Kelvin elements, each characterised by the compliance $D_{jk,i}$ and relaxation time τ_i.

Therefore, the creep compliance master curves of Fig. 7, Figs. B1 and B2 can be independently fitted with the previous expression and employed to obtain the material parameters of the Prony series in the reduced time domain and at the reference temperature $\mathrm{T_{ref}}$, $\boldsymbol{D}(t', \mathrm{T_{ref}})$.

To reach shorter time scales compared to the measured data, the tail of the master curve (shifted compliance values of the tests below 15° C) was extrapolated with a linear fit in the logarithmic time-strain domain of Fig. 7, until a time of 10^{-12} s. These data were included in the fitting process in order to avoid ill-conditioned predictions at lower temperatures and high strain rates. The fitting was performed by imposing the relaxation times τ_i and minimising the error to get the compliance parameters (Bosi and Pellegrino 2018; Li et al. 2016). For each direction $1 \equiv \mathrm{MD}$, $2 \equiv \mathrm{TD}$, $6 \equiv \mathrm{ID}$, twenty-one τ_i were defined, evenly spaced in a logarithmic scale between 10^{-12} and 10^{11} s, resulting in twenty-two free compliance parameters, D_0 and D_i. The solution was found with the least square method, using `fitnlm` function of MATLAB. The boundaries imposed on the free parameters representing the compliance were an order of magnitude distant from the stiffest and the softest

Table 2 Material parameters for ETFE linear viscoelastic constitutive model

	MD	TD	ID
E_a [kJ/mol]	2.57E+05	2.39E+05	2.85E+05
τ [s]	D_{11} [MPa]	D_{22} [MPa]	D_{66} [MPa]
0.00E+00	5.33E−04	5.79E−04	8.75E−04
1.00E−12	2.40E−05	1.98E−05	2.52E−05
1.41E−11	2.41E−05	1.97E−05	2.49E−05
2.00E−10	2.51E−05	2.03E−05	2.55E−05
2.82E−09	2.62E−05	2.10E−05	2.63E−05
3.98E−08	2.73E−05	2.18E−05	2.70E−05
5.62E−07	2.85E−05	2.22E−05	2.78E−05
7.94E−06	2.97E−05	2.38E−05	2.84E−05
1.12E−04	3.12E−05	2.21E−05	2.95E−05
1.58E−03	3.18E−05	2.93E−05	2.94E−05
2.24E−02	3.53E−05	2.08E−05	3.29E−05
3.16E−01	3.13E−05	2.84E−05	2.65E−05
4.47E+00	4.55E−05	3.22E−05	4.21E−05
6.31E+01	3.28E−05	2.40E−05	4.59E−05
8.91E+02	5.34E−05	2.92E−05	5.57E−05
1.26E+04	5.62E−05	6.06E−05	7.63E−05
1.78E+05	1.14E−04	7.15E−05	1.04E−04
2.51E+06	2.20E−04	1.54E−04	1.43E−04
3.55E+07	3.61E−04	3.00E−04	3.92E−04
5.01E+08	6.64E−04	5.00E−04	6.25E−04
7.08E+09	1.01E−03	8.45E−04	1.06E−03
1.00E+11	1.30E−03	1.38E−03	1.83E−03

compliance values recorded in the procedure, for the lower and upper bound, respectively. Table 2 reports the imposed relaxation times and the compliance parameters resulting from the fitting procedure. Figure 8 plots the experimental shifted creep compliance overlaid by the fitting master curve, showing an excellent agreement for the three directions tested, with $R^2 = 0.999$. Moreover, the plots show how the creep compliance master curves along the two material principal directions MD and TD have negligible differences at shorter time scales, while they diverge for longer times, with TD being stiffer than MD. This justifies the choice of an orthotropic constitutive model, and could be a possible explanation for the higher value of orthotropy ratio in the uniaxial tensile test at 60° C, $\dot{\epsilon} = 0.1\%/s$, Sect. 3.2.

To complete the model, it was assumed that $D_{12} = D_{21} = -\nu D_{11}$, where $\nu = 0.43$ is the Poisson's ratio determined from DIC measurements of the transverse strain during the uniaxial tensile tests along MD and TD, described in Sect. 3.2. Slight variations (maximum 7%) of the Poisson's ratio were observed across the whole temperature and strain rate range, whose effects were neglected. Lastly, the variation in the out-of-plane direction can be determined by means of the through-thickness engineering strain $\epsilon_3 = D_{13}\sigma_1 + D_{23}\sigma_2$, where, in the absence of direct measurements of the out-of-plane strain, D_{13} and D_{23} might also be assumed equal to D_{12}. It should be noted that this calculation is not needed for the definition of the plane stress model and the value of the compliances assumed could not be verified in the test campaign of the present study. It is acknowledged that the hypothesis made for D_{13} and D_{23}, although reasonable, could lead to inaccuracies in the through-thickness strain.

Fig. 8 Creep compliance master curves along MD (D_{11}), TD (D_{22}) and ID (D_{66}) reported as a function of the reduce time t'. The creep compliance experimental data at different temperatures, used in the fitting procedure of each Prony series are reported in grey underneath the dotted lines representing the model. (Color figure online)
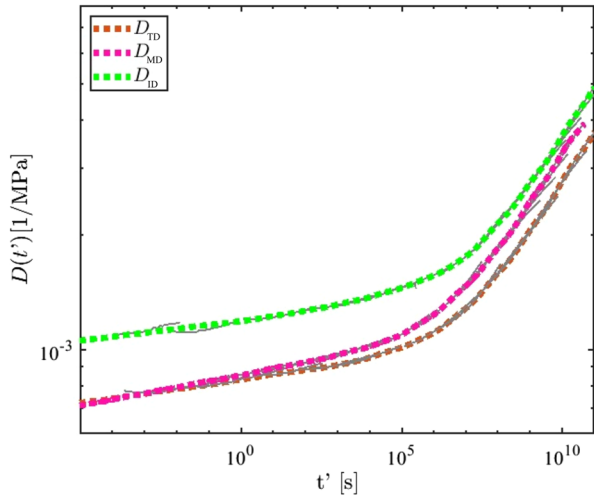
Once the parameters had been identified, Equation (3) was amended to include the time-temperature superposition, allowing its use in a wide range of temperatures and strain rates. If only one generic component of the strain tensor is considered, this results in the expression

$$\epsilon_j(t', T) = \int_0^{t'} \left[D_{jk,0} + \sum_{i=1}^N D_{jk,i} \left(1 - e^{-\frac{t'-s}{\tau_i(T_{\text{ref}})}} \right) \right] \frac{d\sigma_k}{ds} ds, \tag{6}$$

which will be used in the following implementation and validation of the model.

4.2 Numerical implementation and recursive integration algorithm

To validate the constitutive model and implement it into numerical procedures and finite element (FE) packages, the integral viscoelastic relation of Equation (6) needs to be discretised. A convenient choice is to adopt a recursive integration algorithm (Bosi and Pellegrino 2018; Li et al. 2016; Haj-Ali and Muliana 2004). In fact, even if the time integral refers to the whole loading history, the recursive integration algorithm enables obtaining the current strain field only by storing the variables at the previous time step, thus significantly saving computational time and resources. The assumptions underlying the procedure are that *i*) the stress at the initial time step is zero and *ii*) the stress variation is constant across the time step. As a consequence, a suitable time step should be selected to get negligible approximation errors. The constitutive relation that is produced as a numerical equivalent to Equation (6) is

$$\epsilon_j(t') = \tilde{D}_{jk}^{t'} \sigma_k^{t'} - F_j^{t'-\Delta t'}, \tag{7}$$

where $\tilde{D}_{jk}^{t'}$ is the sum of the instantaneous compliance and the transient ones, referred only to the current time step t', while $F_j^{t'-\Delta t'}$ represents the hereditary components, depending on the previous state $t' - \Delta t'$. In particular,

$$\tilde{D}_{jk}^{t'} = D_{jk,0} + \sum_{i=1}^N D_{jk,i} \left(1 - \tau_i \frac{1 - e^{-\frac{\Delta t'}{\tau_i}}}{\Delta t'} \right), \tag{8}$$

and

$$F_j^{t'-\Delta t'} = \sum_{i=1}^{N} D_{jk,i} \left[e^{-\frac{\Delta t'}{\tau_i}} \left(\int_0^{t'-\Delta t'} e^{-\frac{t'-\Delta t'-s}{\tau_i}} \frac{d\sigma_k}{ds} ds \right) - \tau_i \, \sigma_k^{t'-\Delta t'} \left(\frac{1 - e^{-\frac{\Delta t'}{\tau_i}}}{\Delta t'} \right) \right]. \quad (9)$$

The set of Equation (7) along the directions $j, k = \{1, 2, 3, 6\}$ provides the viscoelastic strains once the stress is given as input. To employ the algorithm, it is instrumental to invert Equation (7) to calculate stresses from strain inputs

$$\sigma_j(t') = \Lambda_{jk}^{t'} \left(\epsilon_k^{t'} + F_k^{t'-\Delta t'} \right), \quad (10)$$

where $\Lambda_{jk}^{t'}$ is the jk-th component of the inverse matrix of $\tilde{\boldsymbol{D}}^{t'}$. Additional details on the formulation can be found in literature (Bosi and Pellegrino 2018; Li et al. 2016), where the same notation is used. The algorithm was implemented in a MATLAB code and employed to validate the model against experimental results, as shown in the following section. The MATLAB code and an example of its application can be found at github.com/fbosi/ETFE-constitutivemodel.

4.3 Validation

The model validation is performed by comparing the model predictions with the measured uniaxial tensile data of Sect. 2.2, which were not used in the calibration of the model parameters. In order to simulate the experiments, the time, temperature and strain vectors acquired during the tests were used as input to the algorithm. The predicted stress obtained as output was then compared with the test raw data, as shown in Fig. 9. The plots also report the initial stiffness calculated in Sect. 3.2.

The linear viscoelastic model is shown to predict accurately the material response until ca. 1% of strain at ambient temperature, Fig. 9a. In this case, the influence of the shift factor and TTSP is negligible because the reference temperature T_{ref} is very close to the test condition. The predicted response shows a low level of viscosity, resembling a linear behaviour in a stress-strain graph. This is attributed to the stress level chosen for the creep tests used to build the linear viscoelastic model, which causes limited viscous effects in the time scale of the uniaxial tests. Considering the linearity of the stress-strain simulated output, it is useful to compare the material initial stiffness against the one measured from the experimental data. The discrepancies between the two values are reported in Fig. 9b. On average, the discrepancy amounts to 7%, with peaks at 0° C and 60° C, amounting to 12% and 11%, respectively. Similar results were obtained for TD and ID, as shown in Appendix C.

The ability of the viscoelastic model to capture temperature and strain rate effects through the shift factor is highlighted in Figs. 9c and 9d. At lower temperatures, the variation between the measured and predicted initial modulus E is 7% on average for the tests at $-20°$ C and 0° C. The reduced time t' in the sub-ambient test at $-20°$ C goes beyond the raw data acquired from creep tests for the creation of the master curve and it falls in the extrapolated region. Hence, the choice of the shift factor and an appropriate method of data extrapolation is satisfyingly substituting the missing experimental data at $T < -20°$ C. Furthermore, the shift factor works well also for the experiments carried out at 40° C, with only an average 3% variation in E. At 60° C, the model predicts a stiffer behaviour, with a discrepancy from the measured E of 10%. The highest discrepancies are also observed at 60° C for both TD and ID. They can be attributed to the difficulties of the one-parameter Arrhenius law to capture the material response at temperatures around the secondary transition, as testified by the
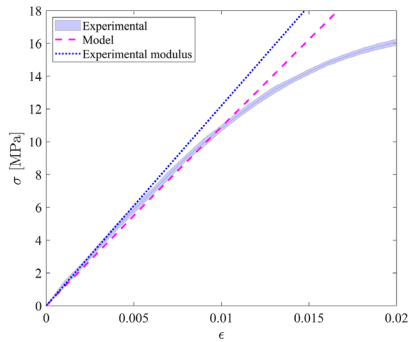
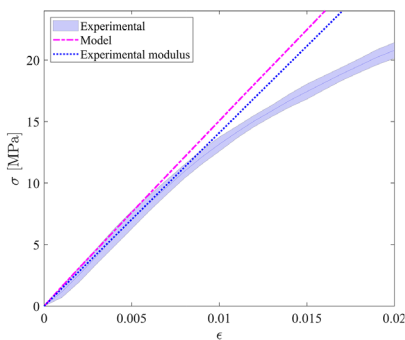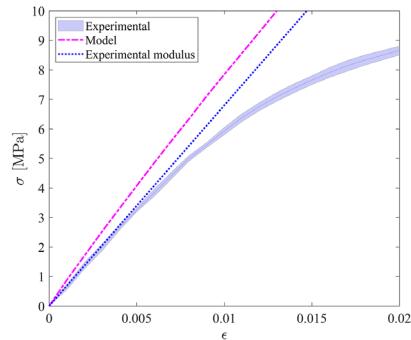(a) T = 20°C, $\dot{\epsilon}$ = 0.1%/s.
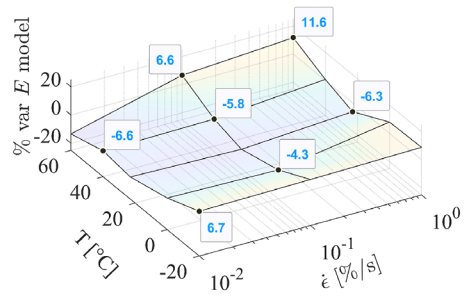
(b) Initial stiffness variation

(c) T = - 20°C, $\dot{\epsilon}$ = 0.1%/s.

(d) T = 60°C, $\dot{\epsilon}$ = 0.1%/s.

Fig. 9 (a, c, d) Comparison between ETFE uniaxial tensile tests and linear viscoelastic model predictions at various temperature and $\dot{\epsilon} = 0.1\%$/s along MD. (b) Percentage difference between the initial modulus E obtained from experimental data and model predictions for all the temperatures and deformation rates considered (the numerical data are reported in Table 3). (Color figure online)

deviation observed in the shift factor regression above 40° C, shown in the inset of Fig. 7. Overall, the model works well in the prediction of the temperature and strain rate-dependent response of the material at small strains. Table 3 reports the initial stiffnesses predicted by the linear viscoelastic model across the range of temperatures and deformation rates investigated, and their percentage variation with respect to the measurements from uniaxial tensile tests. The minor discrepancies are acceptable considering the simple Arrhenius law adopted to model the shift factor, the experimental uncertainty associated with the training and validation data, and the comparison of data acquired with two different experimental setups, namely DMA creep tests and uniaxial tensile experiments.

4.4 Discussion

The linear viscoelastic model is shown to be effective in capturing ETFE uniaxial behaviour at small strains, providing accurate predictions even for stress levels higher than those used in the model calibration. With this model and its numerical implementation through the recursive algorithm, it is also possible to simulate multiaxial stress states. However, when the stress state is approaching the material yield point, the model is not capable of following the

Table 3 Predicted initial stiffness E for uniaxial tensile tests and percentage variation with respect to the experimental data of Table 1

$\dot{\varepsilon}$ [%/s]	T [° C]	E			% var. on experiment		
		MD [MPa]	TD [MPa]	ID [MPa]	MD	TD	ID
0.01	−20	1428.82	1415.82	961.83	6.72	1.38	3.09
	0	1246.1	1248.53	874.78	−2.62	−9.39	−1.74
	23	1040.3	1094.22	804.12	−9.21	−9.87	−2.1
	40	911	972.57	700.93	−6.63	−4.56	4.25
	60	579.24	677.52	520.58	−13.4	−0.08	27.4
0.1	−20	1515.95	1439.75	985.24	7.61	−2.25	2.41
	0	1304.81	1294.67	898.19	−4.31	−7.1	−6.54
	23	1082.71	1129.28	809.84	−11.25	−12.86	−3.25
	40	970.71	1043.38	738.14	−5.76	1.41	7.11
	60	724.45	809.96	617.96	6.56	4.39	22.99
1	−20	1526.07	1410.11	1008.61	8.8	−8.81	7.4
	0	1384.67	1336.64	920.35	7.96	−1.79	1.47
	23	1128.69	1161.67	843.26	−6.25	−8.12	−7.4
	40	1030.75	1081.93	772.5	0.73	−0.92	9.95
	60	881.66	946.32	672.35	11.58	21.49	37

highly nonlinear stress-strain response. For that aim, the model can be extended by including a stress-dependent shift factor and by introducing a nonlinear viscoelastic response.

Nevertheless, the current work is thought to be useful in the design of typical ETFE building constructions where the stress level is kept well below the yield point. The proposed linear viscoelastic model can simulate the time- and temperature-dependent behaviour of ETFE membranes both in creep and relaxation conditions, a crucial aspect in structural engineering applications, such as in inflated cushions, snow loads and single or multiple foils pre-tensioning. These effects can have a dramatic impact on the structural safety of lightweight tensile structures: material relaxation causes a pre-stress loss and a global stiffness reduction, whereas the dual condition of creep causes a time-dependent increase of strain that can approach and surpass yielding. In this regard, an example of the model capability is displayed in Fig. 10, where the results of creep and relaxation tests at different stress levels and temperatures are shown alongside the predicted responses.

Figure 10 shows a very good agreement between the constitutive relation and the independently acquired data, which demonstrate excellent prediction capabilities at higher stress levels compared to those employed in the model development. The main differences observed are related to the initial stiffness, with the highest deviation of 14% obtained for the tests at 60° C in Fig. 10d; this is attributed to the least accurate model prediction at the highest temperature investigated, for the reasons mentioned above. The overall behaviour in time is predicted accurately, except for the test in Fig. 10c. The reason behind the diverging measured and predicted stress responses after ca. 10^3 s is attributed to the material exceeding the limit of the linear viscoelastic region, determined in Sect. 3.3 for the highest temperature in the range of interest. Nonlinear effects are more relevant at high temperatures, while at lower temperatures, the linear viscoelastic domain is more extended (Jiang et al. 2015). The examples in Fig. 10 show four test conditions where the initial stress level is beyond
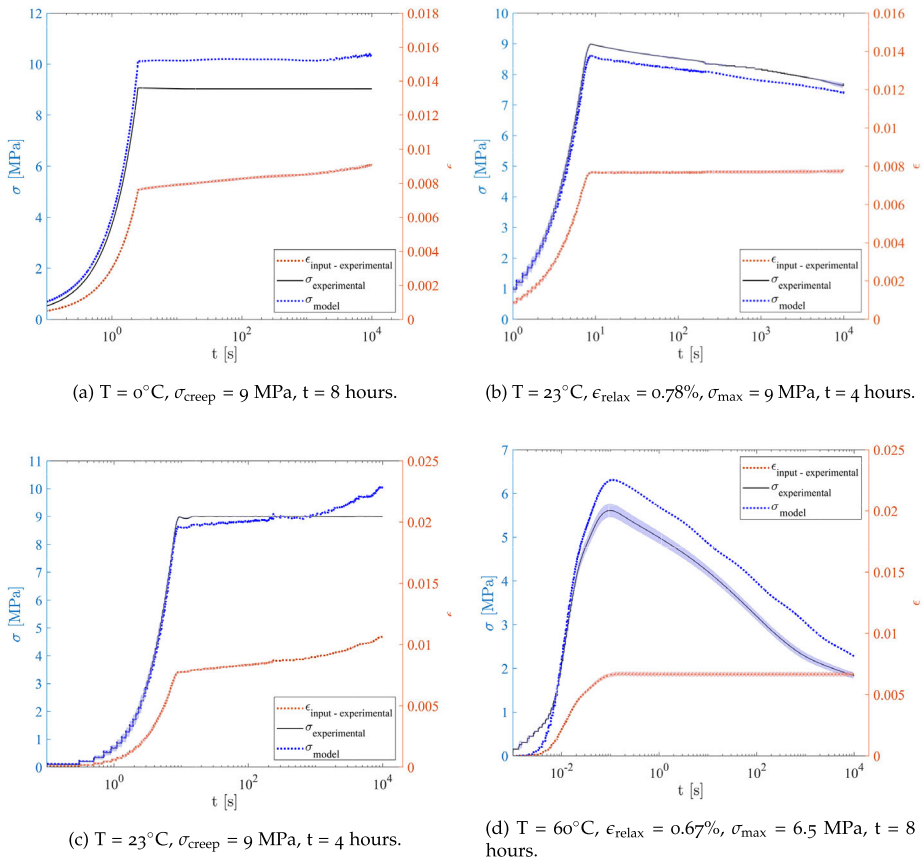
(a) T = 0°C, σ_{creep} = 9 MPa, t = 8 hours.

(b) T = 23°C, ϵ_{relax} = 0.78%, σ_{max} = 9 MPa, t = 4 hours.

(c) T = 23°C, σ_{creep} = 9 MPa, t = 4 hours.

(d) T = 60°C, ϵ_{relax} = 0.67%, σ_{max} = 6.5 MPa, t = 8 hours.

Fig. 10 Comparison between uniaxial creep (a, c) and relaxation (b, d) test data and predicted model response along MD, at different temperatures. (Color figure online)

the onset of the nonlinear viscoelastic phase of the stress-strain curve, if compared with the data reported in Fig. 5. The accuracy of the predictions indicates the suitability of the linear viscoelastic model also outside its training bounds, at least for some loading conditions. In particular, relaxation conditions favour the accuracy of the model because they cause the stress to decrease at a negative strain rate: the nonlinear effects, if existing, lose relevance during this process. In fact, it can be observed in both the relaxation tests at 23° C and 60° C (Figs. 10b and 10d, respectively) that, despite the stress level being relatively close to the inflection point, the behaviour over time is captured well. On the other hand, in creep conditions, the stress is constant and the nonlinear effects persist while the material continues to strain. If the stress level is sufficiently high, such that the material enters the nonlinear viscoelastic regime, the linear model is unable to correctly predict the response. This explains the deviation of the predicted response for the creep test at 23° C in Fig. 10c, while at the same stress level and 0° C the predicted and measured responses in Fig. 10a show an excellent agreement. Additionally, the low strain rate of the creep condition causes the yield surface to shrink, as observed for ETFE and other structural polymeric membranes (Bosi and Pellegrino 2017). Therefore, the model prediction under creep conditions might lose accuracy over time and underestimate the real response because the material could reach

the onset of plasticity. As a consequence, the use of the proposed model should be carefully evaluated when the creep stress is sufficiently close to the yield strength. Although the limits of the developed linear viscoelastic model depend on time and temperature effects, a reasonable boundary of applicability can be considered 1% of equivalent engineering strain, as suggested in Sect. 4.3. This threshold is considered satisfactory when relating it to the use of ETFE membranes in building applications, especially considering the Serviceability Limit State (SLS) design. The proposed linear viscoelastic model could represent a useful tool in predicting and evaluating several aspects of the design of tensile structures, such as stress relaxation occurring in the installation phase of the membrane and creep strain resulting from moderate snow or rainfall.

It should be noted that the model presented was fitted only on one product and thickness available on the market. Other studies have highlighted different mechanical responses between ETFE foils with various thicknesses and produced by different manufacturers (Surholt et al. 2022; De Focatiis and Gubler 2013). Hence, the developed model might not accurately predict the behaviour of other ETFE foils, or it would need to be re-scaled with appropriate experimental-based factors (Cabello and Bown 2019). However, the presented characterisation procedure, constitutive model and implementation are readily applicable to the development of linear viscoelastic models for other polymeric foils.

5 Conclusion

A thermomechanical characterisation of ETFE foils was performed to assess the influence of temperature, strain rate and material orientation on the viscous material response. ETFE was found to be slightly orthotropic and in a glassy phase across the temperature range of interest. The understanding of the boundaries of the linear viscoelastic region, obtained through creep test isochrones, allowed the application of the time-temperature superposition principle in the creation of experimental creep compliance master curves for the two principal directions of the material, MD and TD, and the shear response. The master curves enable the prediction of the linear viscoelastic response in a wide range of temperatures and time scales, much longer than that obtainable in laboratory tests, through the time shift factor defined by the Arrhenius law. Subsequently, the creep compliance curves were employed in defining a plane stress orthotropic linear viscoelastic model, which was numerically implemented using a recursive integration algorithm. The vast set of experiments carried out along MD, TD and ID directions allowed to perform the validation of the model on independently acquired data, which yielded good results across the range of temperature of interest in building applications, $-20°$ C to $60°$ C, two orders of magnitude of deformation rates, 0.01%/s to 1%/s, various tensile tests, creep and relaxation conditions. The proposed constitutive law is shown to help predict typical load conditions for the engineering design of ETFE structures. Nevertheless, if larger strains ($>1\%$), nonlinearities and material hardening want to be exploited in non-standard designs, the results have also highlighted the need for a comprehensive orthotropic nonlinear viscoelastic and viscoplastic model, which will be part of future developments.

Appendix A: Uniaxial tensile tests results along TD and ID

The results of the uniaxial tensile tests at various temperatures and strain rates performed along TD and ID are displayed in Figs. A1 to A4, analogous to those presented in Figs. 4 and 5.

Fig. A1 Strain rate effects on ETFE engineering stress-strain curve, at $T_{amb} = 23°$ C and along TD. The inset shows the percentage variation of the initial stiffness E with respect to that at the reference strain rate 0.1%/s across the temperature range. The solid line represents the average value, while the coloured area is the standard deviation. (Color figure online)
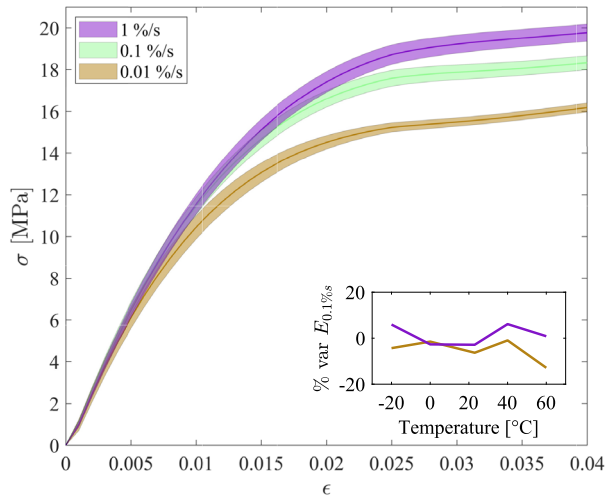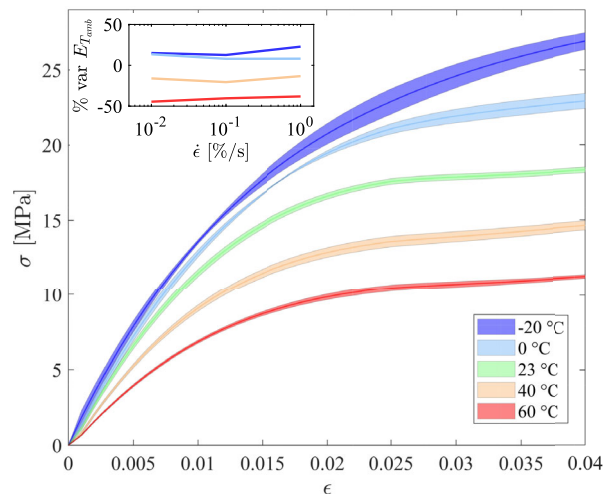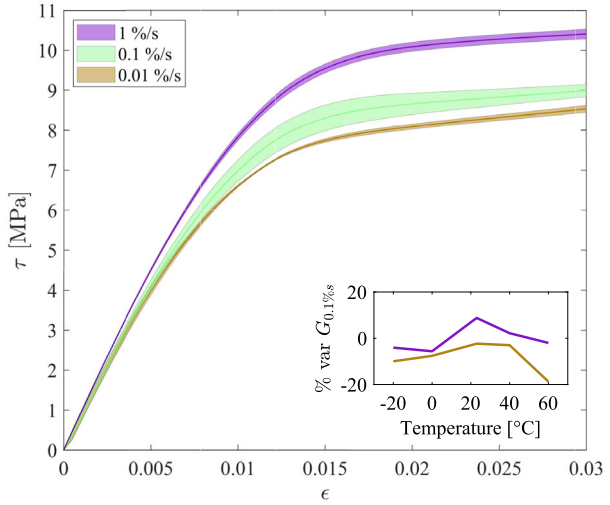
Fig. A2 Temperature effects on ETFE engineering stress-strain curve for uniaxial tests performed at 0.1%/s along TD. The inset shows the percentage variation of the initial stiffness E with respect to that at T_{amb} across the strain rate range. The solid line represents the average value, while the coloured area is the standard deviation. (Color figure online)

Fig. A3 Strain rate effects on ETFE engineering stress-strain curve, at $T_{amb} = 23°$ C and along ID. The inset shows the percentage variation of the initial stiffness E with respect to that at the reference strain rate 0.1%/s across the temperature range. The solid line represents the average value, while the coloured area is the standard deviation. (Color figure online)

Fig. A4 Temperature effects on ETFE engineering stress-strain curve for uniaxial tests performed at 0.1%/s along ID. The inset shows the percentage variation of the initial stiffness E with respect to that at T_{amb} across the strain rate range. The solid line represents the average value, while the coloured area is the standard deviation. (Color figure online)
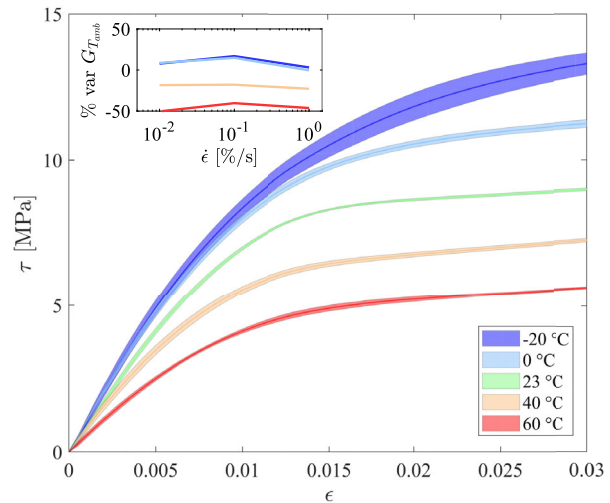
Appendix B: Creep compliance master curves of TD and ID

The experimental creep compliance master curves created for the direction TD and ID by horizontally shifting the creep compliance tests performed at different temperatures, as described in Sect. 3.1, are displayed in Figs. B1 and B2.
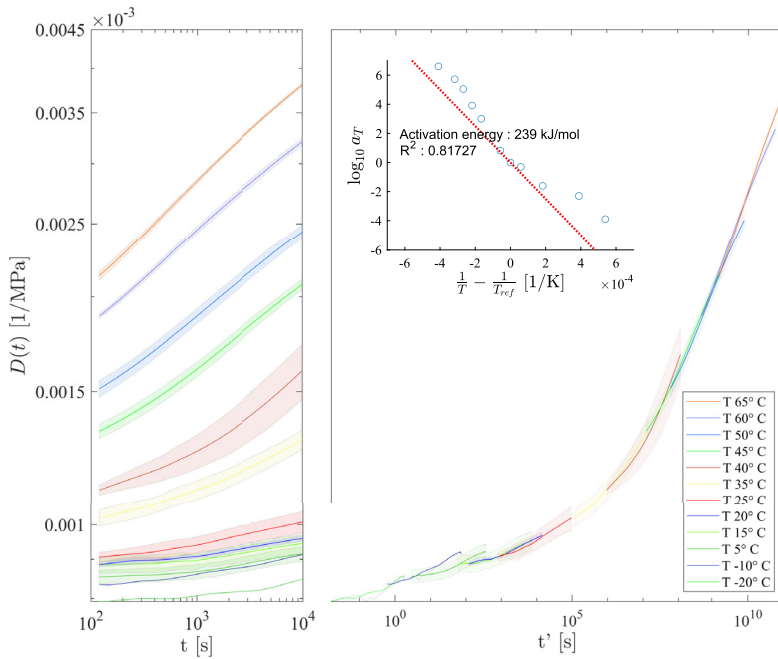
Fig. B1 Left: engineering creep compliance at different temperatures from creep test performed at $\sigma_0 = 1.5$ MPa along TD. Right: Engineering creep compliance master curves along TD at $T_{ref} = 20°$ C, obtained by horizontally shifting the compliance curves at other temperatures through the time shift factor a_T. The inset shows the experimental shift factors and their fitting through the Arrhenius law. (Color figure online)
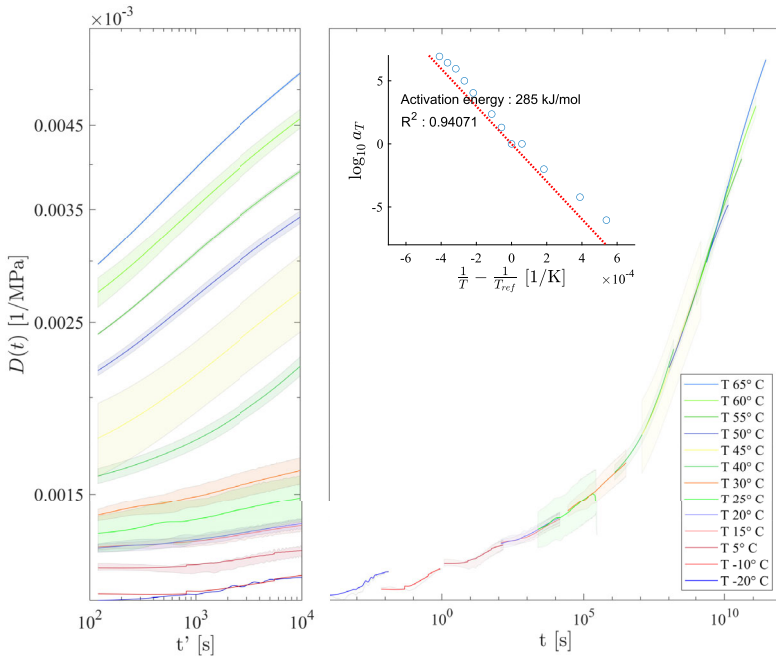
Fig. B2 Left: engineering creep compliance at different temperatures from creep test performed at $\tau_0 = 0.75$ MPa along ID. Right: Engineering creep compliance master curves along ID at $T_{ref} = 20°$ C, obtained by horizontally shifting the compliance curves at other temperatures through the time shift factor a_T. The inset shows the experimental shift factors and their fitting through the Arrhenius law. (Color figure online)

Appendix C: Model validation

Figures C1 and C2 report the comparison between the model predictions and the measured data for uniaxial tensile tests at different temperatures and strain rates for TD and ID respectively. The results are analogous to those displayed for MD in Fig. 9.

Figure C3 represent respectively the a, c, and d subplots of Fig. 9, Fig. C1 and Fig. C2 combined in one common plot. The results show the high influence of temperature on ETFE response and the accurate model prediction until $\epsilon \approx 1\%$.

(a) T = 20°C, ἐ = 0.1%/s.

(b) Initial stiffness variation

(c) T = -20°C, ἐ = 0.1%/s.
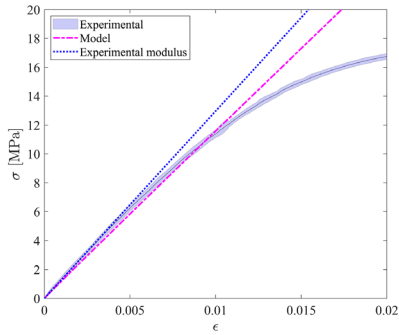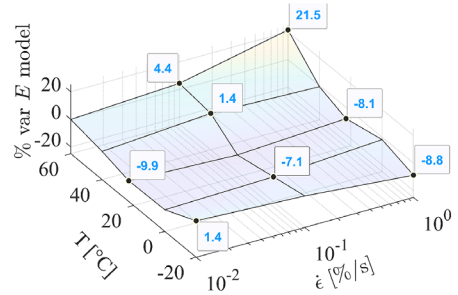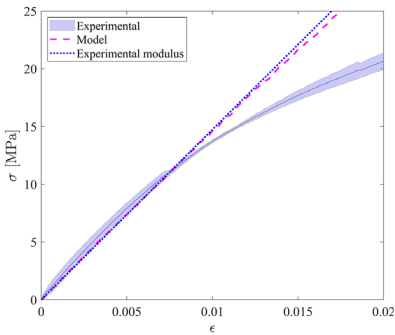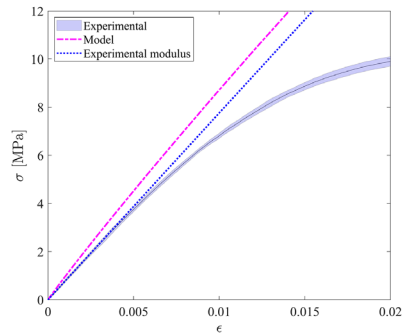
(d) T = 60°C, ἐ = 0.1%/s.

Fig. C1 (a, c, d) Comparison between ETFE uniaxial tensile tests and linear viscoelastic model predictions at various temperature and ἐ = 0.1%/s along TD. (b) Percentage difference between the initial modulus E obtained from experimental data and model predictions for all the temperatures and deformation rates considered (the numerical data are reported in Table 3). (Color figure online)
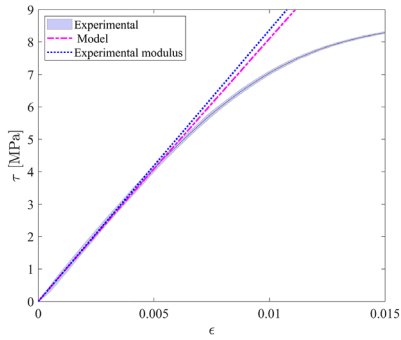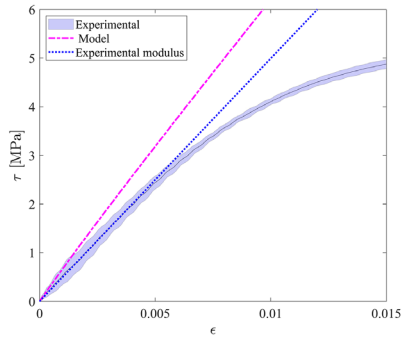
(a) T = 20°C, $\dot{\epsilon}$ = 0.1%/s.
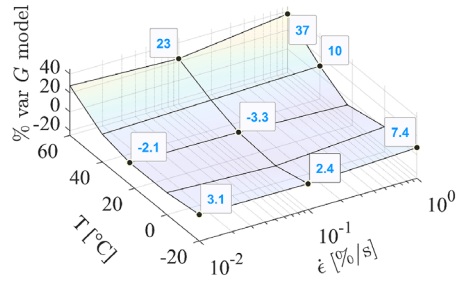
(b) Initial stiffness variation
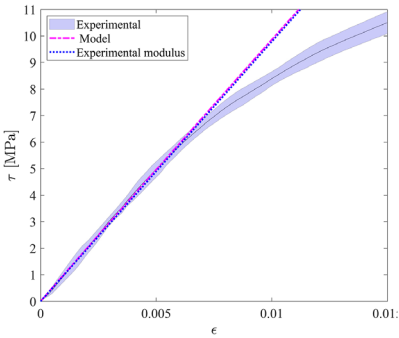
(c) T = -20°C, $\dot{\epsilon}$ = 0.1%/s.

(d) T = 60°C, $\dot{\epsilon}$ = 0.1%/s.

Fig. C2 (a, c, d) Comparison between ETFE uniaxial tensile tests and linear viscoelastic model predictions at various temperature and $\dot{\epsilon}$ = 0.1%/s along ID. (b) Percentage difference between the initial modulus E obtained from experimental data and model predictions for all the temperatures and deformation rates considered (the numerical data are reported in Table 3). (Color figure online)

(a) MD

(b) TD

(c) ID
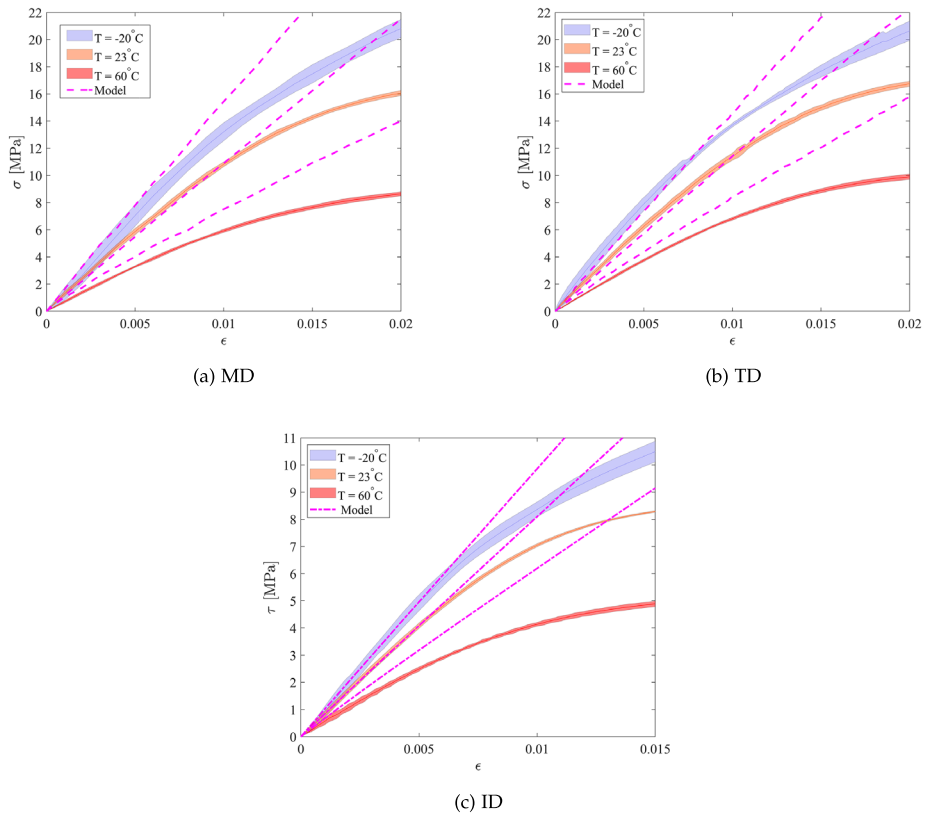
Fig. C3 Comparison between ETFE uniaxial tensile tests and linear viscoelastic model predictions (dasjed lines) at $T = -20°$ C, $T_{amb} = 23°$ C, and $T = 60°$ C, at $\dot{\epsilon} = 0.1\%/s$, along MD (a), TD (b), ID (c). The solid line represents the average experimental value, while the coloured area is the standard deviation. (Color figure online)

Author contributions A.C. performed the experiments, developed the model formulation and the numerical implementation and wrote the draft paper. F.B. conceptualized and supervised the research, provided theoretical and experimental guidance, and contributed to the final version of the paper.

Data availability No datasets were generated or analysed during the current study.

Code availability The MATLAB code containing the recursive algorithm to use the linear viscoelastic model and examples of its application can be found at github.com/fbosi/ETFEconstitutivemodel.

Declarations

Competing interests The authors declare no competing interests.

References

Arrhenius, S.: Über die Reaktionsgeschwindigkeit bei der Inversion von Rohrzucker durch Säuren. Z. Phys. Chem. **4U**, 226–248 (1889)

Beck, P.: Zum zeit- und temperaturabhängigen werkstoffverhalten von ethylen tetrafluorethylen-folien im hochbau. PhD thesis, Technische Universität Darmstadt (2021)

Bosi, F., Pellegrino, S.: Molecular based temperature and strain rate dependent yield criterion for anisotropic elastomeric thin films. Polymer **125**, 144–153 (2017). https://doi.org/10.1016/j.polymer.2017.07.080

Bosi, F., Pellegrino, S.: Nonlinear thermomechanical response and constitutive modeling of viscoelastic polyethylene membranes. Mech. Mater. **117**, 9–21 (2018). https://doi.org/10.1016/j.mechmat.2017.10.004

Brinson, H.F., Brinson, L.C.: Polymer Engineering Science and Viscoelasticity: An Introduction. Springer, New York (2008). OCLC: ocn172979443

Brooks, N.W., Duckett, R.A., Ward, I.M.: Investigation into double yield points in polyethylene. Polymer **33**(9), 1872–1880 (1992). https://doi.org/10.1016/0032-3861(92)90486-G

Cabello, A., Bown, A.C.: Using a nonlinear thermo-viscoelastic constitutive model for the design and analysis of ETFE structures. In: Proceedings of the IASS Annual Symposium 2019, Barcellona, p. 18 (2019)

Comitti, A., Vijayakumaran, H., Nejabatmeimandi, M.H., Seixas, L., Cabello, A., Misseroni, D., Penasa, M., Paech, C., Bessa, M., Bown, A.C., Dal Corso, F., Bosi, F.: In: Bahrami, A. (ed.) Ultralight Membrane Structures Toward a Sustainable Environment, pp. 17–37. Springer, Cham (2024). https://doi.org/10.1007/978-3-031-46688-5_2

D11 Committee: Test Methods for Vulcanized Rubber and Thermoplastic ElastomersTension. Technical report, ASTM International (2021). https://doi.org/10.1520/D0412-16R21

De Focatiis, D.S.A., Gubler, L.: Uniaxial deformation and orientation of ethylene–tetrafluoroethylene films. Polym. Test. **32**(8), 1423–1435 (2013). https://doi.org/10.1016/j.polymertesting.2013.09.007

European Commission, Joint Research Centre, Stranghöner, N., Uhlemann, J., Bilginoglu, F., et al.: Prospect for European guidance for the structural design of tensile membrane structures. Other KJ-NA-31-430-EN-N (online), KJ-NA-31-430-EN-C (print), Luxembourg (Luxembourg) (2023). https://doi.org/10.2760/24763 (online), https://doi.org/10.2760/335999 (print)

Fesko, D.G., Tschoegl, N.W.: Time-temperature superposition in thermorheologically complex materials. J. Polym. Sci., C Polym. Symp. **35**(1), 51–69 (2007). https://doi.org/10.1002/polc.5070350106

Galliot, C., Luchsinger, R.H.: Uniaxial and biaxial mechanical properties of ETFE foils. Polym. Test. **30**(4), 356–365 (2011). https://doi.org/10.1016/j.polymertesting.2011.02.004

Haj-Ali, R.M., Muliana, A.H.: Numerical finite element formulation of the schapery non-linear viscoelastic material model. Int. J. Numer. Methods Eng. **59**(1), 25–45 (2004)

Houtman, R.: TensiNet European Design Guide for Tensile Structures. Appendix 5: Design recommendations for ETFE foil structures. TensiNet Association, Brussel (2013)

Hu, J., Chen, W., Zhao, B., Wang, K.: Uniaxial tensile mechanical properties and model parameters determination of ethylene tetrafluoroethylene (ETFE) foils. Constr. Build. Mater. **75**, 200–207 (2015). https://doi.org/10.1016/j.conbuildmat.2014.10.017

Hu, J., Chen, W., Zhao, B., Yang, D.: Buildings with ETFE foils: a review on material properties, architectural performance and structural behavior. Constr. Build. Mater. **131**, 411–422 (2017). https://doi.org/10.1016/j.conbuildmat.2016.11.062

Jiang, C., Jiang, H., Zhu, Z., Zhang, J., Guo, S., Xiong, Y.: Application of time-temperature-stress superposition principle on the accelerated physical aging test of polycarbonate. Polym. Eng. Sci. **55**(10), 2215–2221 (2015). https://doi.org/10.1002/pen.24106

Karwath, M., Wagner, R., Kröplin, B.: Ein orthotropes werkstoffgesetz für folien. Stahlbau **76**(5), 297–304 (2007)

Li, Y., Wu, M.: Uniaxial creep property and viscoelastic–plastic modelling of ethylene tetrafluoroethylene (ETFE) foil. Mech. Time-Depend. Mater. **19**(1), 21–34 (2015). https://doi.org/10.1007/s11043-014-9248-2

Li, J., Kwok, K., Pellegrino, S.: Thermoviscoelastic models for polyethylene thin films. Mech. Time-Depend. Mater. **20**, 13–43 (2016). https://doi.org/10.1007/s11043-015-9282-8

Schapery, R.A.: On the characterization of nonlinear viscoelastic materials. Polym. Eng. Sci. **9**(4), 295–310 (1969). https://doi.org/10.1002/pen.760090410

Solutions, C.: VIC-3D software manual (2019)

Stranghöner, N., Uhlemann, J., Bilginoglu, F., Bletzinger, K.-U., Bögner-Balz, H., Corne, E., Gibson, N., Gosling, P., Houtman, R., Llorens, J., Malinowsky, M., Marion, J.-M., Mollaert, M., Nieger, M., Novati, G., Sahnoune, F., Siemens, P., Stimpfle, B., Tanev, V., Thomas, J.-C.: Prospect for European guidance for the structural design of tensile membrane structures. Technical report (2016). https://doi.org/10.2788/967746

Sun, G., Wu, M., Qu, X., Xue, S.: Experimental investigation of the uniaxial tensile properties and thermal deformation of the ETFE membrane at different temperatures. Constr. Build. Mater. **327**, 126944 (2022). https://doi.org/10.1016/j.conbuildmat.2022.126944

Surholt, F., Uhlemann, J., Stranghöner, N.: Temperature and strain rate effects on the uniaxial tensile behaviour of ETFE foils. Polymers **14**(15), 3156 (2022). https://doi.org/10.3390/polym14153156

Sutton, M.A., Orteu, J.J., Schreier, H.: Image Correlation for Shape, Motion and Deformation Measurements: Basic Concepts, Theory and Applications. Springer, Berlin (2009)

Ward, I.M.: Mechanical Properties of Solid Polymers, p. 396 (2013)

Wong, W., Pellegrino, S.: Wrinkled membranes I: experiments. J. Mech. Mater. Struct. **1**(1), 3–25 (2006)

Yoshino, T., Kato, S.: Formulation of non-linear incremental constitutive equation of ETFE film structure considering the dependence on temperature change. In: Proceedings of the International Association for Shell and Spatial Structures (IASS) Symposium 2013, Wroclaw University of Technology, Poland, p. 5 (2013)

Yoshino, T., Kato, S.: Viscous characteristics of ETFE film sheet under equal biaxial tensions. Proc. Eng. **155**, 442–451 (2016). https://doi.org/10.1016/j.proeng.2016.08.047

Yoshino, T., Kato, S.: Viscous characteristics of ETFE film sheet under temperature change. In: VIII International Conference on Textile Composites and Inflatable Structures, p. 12 (2017)

Yoshino, T., Kato, S.: Viscous characteristics near the initial yield stress of ETFE film sheet under biaxial tension and temperature change. In: Proceedings of the IASS Annual Symposium 2019, Barcellona, p. 8 (2019)